THE JOURNAL OF PHYSICAL CHEMISTRY B

pubs.acs.org/JPCB Article

Oligo(L-glutamic acids) in Calcium Phosphate Precipitation: Chain Length Effect

Putu Ustriyana, Emma Harmon, Kexun Chen, F. Marc Michel, and Nita Sahai*

Cite This: J. Phys. Chem. B 2020, 124, 6278–6287 Read Online

ACCESS | Metrics & More | Article Recommendations | Supporting Information

ABSTRACT: The understanding of calcium phosphate precipitation is of major interest in different fields of science, including medicine, biomaterials, and physical chemistry. The presence of additive biomacromolecules has been known to influence various stages of the precipitation process from nucleation to crystal growth. In the current work, well-defined sequences of short, negatively charged peptides, oligo(L-glutamic acids), were utilized as a model, inspired by contiguous sequences of acidic amino acids in natural biomineralization proteins. The precipitate morphology and phases, the element time profile in solution and in the precipitates, as well as the kinetics during the precipitation process were analyzed to explain the effect of these short peptides on calcium phosphate precipitation. The results show that peptides can delay the phase transformation of an amorphous precursor phase to hydroxyapatite and that there is an optimal chain length for this effect at a given concentration of peptide. This study is the first part of a two-part series and is followed by a subsequent work to reveal the mechanism by which these short peptides influence the calcium phosphate precipitation.

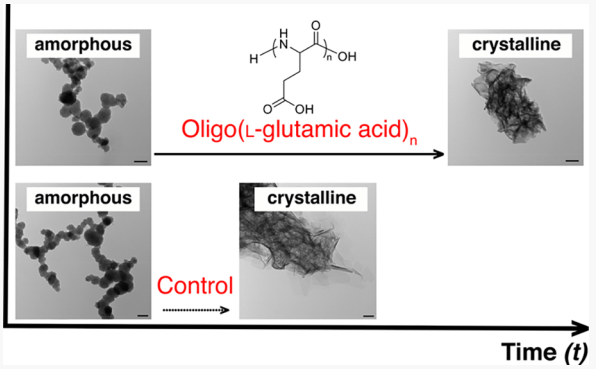

1. INTRODUCTION

The control of the precipitation of calcium phosphate minerals has been a major interest in medicine and industry, especially in the field of dental and orthopedic materials. The understanding of the fundamental mechanism of calcium phosphate nucleation and growth is of importance in revealing normal and pathological mineralization mechanisms. In bone and dental tissue engineering, the treatment approach has been directed toward the application of biomimetic scaffolds with calcium phosphate fillers or bioinert implants that are surface-modified by coating bioactive calcium phosphate minerals.[1−6] Moreover, the study of organic−inorganic interactions at interfaces or in solutions and understanding their mechanisms is of great importance in the area of physical chemistry.

Calcium phosphates are the primary inorganic components in vertebrate mineralized tissue such as bone and teeth. In the biomineralization of these tissues, the nucleation and growth of calcium phosphates is closely associated with biomacromolecules and occurs within an organic matrix of type I collagen.[7−9] Additionally, acidic noncollagenous proteins, rich in negatively charged sequences of amino acid residues, are believed to play a significant role in mediating the mineral formation.[9,10] The precise interaction between the inorganic and organic components of the tissues is key in the formation of mechanically excellent materials with well-controlled mineral phase, shape, and size.[7−10]

Calcium phosphate precipitation in neutral or basic aqueous media starts with the formation of amorphous calcium phosphate (ACP).[11−15] The composition of this amorphous phase depends on the experimental conditions, but literature suggests that the initial ACP cluster is spherical $Ca_9(PO_4)_6$.[16] These clusters may then transform into different phases of calcium phosphate crystals (i.e., octacalcium phosphate [OCP, $Ca_8(HPO_4)_2(PO_4)_4{\cdot}5H_2O$] or hydroxyapatite [HAP, $Ca_{10}(PO_4)_6(OH)_2$], depending on the concentrations of the reactants and the pH of the solutions.[16−18] The presence of organic molecules may change any of these processes and consequently affect the resulting precipitates.

Several studies have shown how biogenic macromolecules are able to control, either by inhibiting or promoting, crystallization of calcium phosphate.[10] In bone biomineralization especially, many studies have looked into aspartic acid- or glutamic acid-rich proteins, such as osteopontin and bone sialoprotein.[19−22] Other groups have focused on investigating the mimics of these proteins on the precipitation of calcium phosphates by using polyglutamic or polyaspartic acids, or model carboxylic acid-rich polymers.[23−29] These studies, however, do not take into account that there is only a specific

Received: February 26, 2020
Revised: June 15, 2020
Published: June 29, 2020

https://dx.doi.org/10.1021/acs.jpcb.0c01689
J. Phys. Chem. B 2020, 124, 6278−6287

number of repeating units (a short segment) of glutamic or aspartic acids in the biogenic proteins. In bone sialoprotein, for example, there are only 8−10 contiguous glutamic acid residues that have been proposed to play a role in HAP mineralization.[19]

Investigations on short homooligopeptide sequences of acidic proteins and their interactions with minerals have been conducted in calcium oxalate and calcium carbonate systems.[30,31] With regard to calcium phosphates, most work using polypeptides is limited to the use of commercially available polymers with relatively high polydispersity and molar mass.[23,24,28] The molecular weight of organic additives is an important factor in modifying various stages of precipitation. In the case of calcium oxalate, for example, the effect of molecular weight can dramatically change the induction period of precipitation by up to a factor of 11 compared to the inorganic control group.[30] Different lengths of polyanions will carry different numbers of functional groups, possibly influencing the electrostatic interactions between the organic additives and ions present in solutions. In addition, polypeptides may adsorb onto the surface of growing precipitates, thus potentially influencing crystal growth. The size of the peptides will also change their binding energy with ions or on the particle surface. In this case, the high polydispersity of polypeptide chains might alter the precipitation results drastically, which presents uncertainties in determining the effects of molecular weight or chain length in precipitation process. Hence, there remains a significant challenge to elucidate the exact mechanism of interaction between calcium phosphates and homooligopeptides with high purity.

The current work is the first of a two-part study series.[32] We aim to provide a systematic investigation on the effects of well-defined sequences of short, negatively charged peptides, oligo(L-glutamic acids), on the precipitation of calcium phosphate. Glutamic acid oligopeptides with four different numbers of repeating units (Glu_3, Glu_7, Glu_8, and Glu_{10}) were used at different concentrations as organic additives in the precipitation of calcium phosphate. We utilized various analytical techniques to characterize the precipitate morphology and phases, and to determine the element time profiles in solution and in the precipitates, as well as the kinetics during the precipitation process. Here, we obtain results showing that there is a critical chain length at which glutamic acid peptides can influence calcium phosphate mineralization, specifically delaying the phase transformation of ACP to HAP. We also show that there is a critical concentration for a peptide of a given length to show this retardation effect.

2. EXPERIMENTAL SECTION

Oligo(L-glutamic acids) were obtained from GenScript (Piscataway, NJ). The purity of the peptides used in the experiments was >95%. All other chemicals were purchased from Sigma-Aldrich (St. Louis, MO) at the highest available purity, and used without further purification. All solutions were prepared with ultrapure deionized water with a resistivity of 18.2 MΩ·cm (Barnstead GenPure xCAD Plus, Thermo Scientific, Rockford, IL) and were filtered through 0.1 μm membranes prior to experiments.

2.1. Precipitation Experiments. Stock solutions of calcium and phosphate of 50 mM concentration were prepared by dissolving $CaCl_2$ and $(NH_4)_2HPO_4$ in 10 mM HEPES buffer (pH 7.4). Oligo(L-glutamic acid) peptides containing 3, 7, 8, and 10 units (Glu_3, Glu_7, Glu_8, and Glu_{10}) were used. 5 mM stock solution of oligo(L-glutamic acid) was prepared by dissolving each peptide in HEPES buffer (10 mM, pH 7.4). For the control group, calcium stock solution was dissolved in HEPES buffer (10 mM, pH 7.4) to reach a concentration of 4 mM. Subsequently, phosphate stock solution was added dropwise (80 $\mu L \cdot min^{-1}$) to reach a concentration of 2.4 mM. For the experimental groups with peptide, the stock solution of peptide was added before the addition of phosphate solution to yield a peptide concentration of 0.1 or 0.5 mM. The resulting mixture was then vortexed briefly and left to age. The precipitation experiments were conducted at room temperature (25 ± 0.2 °C) with no stirring in different sizes of plastic tubes depending on which subsequent characterization technique was to be conducted. Different volumes of suspension were prepared for each characterization technique as explained in detail below.

2.2. Characterization of the Precipitate. *2.2.1. Transmission Electron Microscopy (TEM).* Calcium phosphate suspension of 500 μL was prepared with and without peptides, following the above-described method. Aliquots of 7 μL were extracted from the suspension at different time points (2 min, 10 min, 30 min, 1 h, 3 h, 5 h, 8 h, and 1 day) and dropped onto a Formvar/carbon film-supported copper grid (300 mesh, Ted Pella, Inc., Redding, CA). After 3 min, the liquid was blotted gently with filter paper, and the grid was air-dried overnight. The grid was then visualized under TEM (JEOL JSM-1230, 120 kV, Peabody, MA and FEI Tecnai G2 F20, 200 kV, Hillsboro, OR) to obtain images and selected area electron diffraction (SAED) patterns.

2.2.2. Powder X-ray Diffraction and Small-Angle X-ray Scattering (pXRD and SAXS). To prepare the precipitate for X-ray scattering analysis, calcium phosphate suspensions (see section 2.1) at different time points were centrifuged to separate the solid precipitate (4000 rpm, 5 min). The precipitate was then washed with cold water before being lyophilized. Powder XRD and SAXS data were obtained using an Empyrean Nano Edition multipurpose diffractometer (Malvern Panalytical, Westborough, MA) equipped with a Cu source (λCu Kα = 0.15406 nm) and W/Si elliptic focusing mirror with a 1/32° fixed slit. Dry precipitates for both scattering experiments were flat-mounted between Mylar film and measured under vacuum in a ScatterX78 sample stage. Diffracted intensities from the samples for both pXRD and SAXS were collected using a GaliPIX3D area detector system. SAXS and pXRD intensities were measured from −0.15° to 6° and 5° to 75° 2θ, respectively, at 0.014° increments and exposure time of 138 s/step. Background subtraction and volume-weighted size distribution (Dv(R)) analysis of the SAXS data for each sample was performed in EasySAXS (Malvern Panalytical). Identification of the Bragg peaks associated with (nano)crystalline calcium phosphate phases was performed in HighScore (Malvern Panalytical).

2.2.3. Synchrotron Total X-ray Scattering and Pair Distribution Function (PDF) Analysis. Collection of synchrotron total X-ray scattering for PDF analysis took place at sector 11 beamline ID-B of the Advanced Photon Source at Argonne National Laboratory (Argonne, IL). Dry powder samples were loaded individually into 1 mm O.D. Kapton capillary tubes (Cole-Parmer, Vernon Hills, IL) and sealed with epoxy. The scattered intensities were collected using an amorphous silicon 2D detector system (PerkinElmer, Waltham, MA) at an incident X-ray energy of 58.66 keV (λ = 0.2113 Å). Additional details regarding instrument calibration, data processing, and

https://dx.doi.org/10.1021/acs.jpcb.0c01689
J. Phys. Chem. B 2020, 124, 6278−6287

PDF extraction procedures were reported previously.[33] For data analysis, the composition of the sample was assumed to be ACP and HAP. To yield the reduced PDF, $G(r)$, a Fourier transform of $Q[S(Q)^{-1}]$ was performed using a maximum q value of approximately 23 Å^{-1}.

The quantification of the degree of phase transformation was obtained from linear combination fitting (LCF) of PDF data. The phase abundance was estimated using two components representing ACP (group with 0.18 mM Glu_{10} at 1 h) and crystalline calcium phosphate minerals (inorganic control group at 3 h). The abundances were normalized to 100% and the estimated errors were approximately ±5%.

2.3. Solution Analysis. *2.3.1. Inductively Coupled Plasma-Optical Emission Spectroscopy (ICP-OES).* The concentration of Ca and P in solution, and the ratio of the elements in the resulting precipitate over time were determined using ICP-OES. A total volume of 4 mL calcium phosphate suspensions was prepared (section 2.1). At different time points (2 min, 10 min, 30 min, 1 h, 3 h, 5 h, 8 h, 10 h, and 1 d), 280 μL aliquots were extracted from the suspension and then centrifuged at 15,000 rpm for 5 min. 190 μL of the supernatant and the sedimented precipitate was then separately dissolved in 5% (v/v) nitric acid solution for the measurement of Ca and P concentration using ICP-OES (ICP-OES 720, Agilent, Santa Clara, CA). The concentration of Ca and P was measured at their respective wavelengths of 396.847 and 213.618 nm (the average of three replicates is reported).

2.3.2. Calcium Ion (Ca^{2+})-Selective Electrode. The calcium ion concentration in situ was measured using Ca^{2+}-selective electrode (perfectION Combined Ion-Selective Electrode, Mettler Toledo, Columbus, OH). Calcium phosphate suspension (5 mL) was prepared with or without peptide with the addition of 100 μL of ionic strength adjustment solution (perfectION calcium ISA, Mettler Toledo). The decrease of calcium-ion concentration was observed by a pH/ion meter (SevenCompact S220, Mettler Toledo) and the data were recorded every 15 s (EasyDirect Software, Mettler Toledo). The calcium concentration reported was normalized to the maximum value of each measurement.

2.4. Kinetics Analysis. The change in calcium ion concentration in solution as a function of time, obtained in section 2.3.2, was used to estimate precipitation kinetics. The induction time at which the initial ACP phase transforms into crystalline phase was determined from the tangent intersection between the linear fit to the region at which only a small concentration decrease occurs and a second linear fit to the region where a fast decrease of calcium concentration occurs. To get the rate of crystal transformation and growth, the data were evaluated using a modification of the "derivative method" described by Fischer et al.[30] The use of an empirical fitting procedure has been described in previous studies, especially in analyzing experimental data of a nonseeded system. The experimental concentration values starting from the maximum value of each measurement were fit to a sixth-order polynomial in time:

$$c(t) = A_0 + A_1 t + A_2 t^2 + A_3 t^3 + A_4 t^4 + A_5 t^5 + A_6 t^6 \quad (1)$$

The rate of de-supersaturation (r) was determined as the derivative of the above fit

$$r = \frac{dc(t)}{dt} = A_1 + 2A_2 t + 3A_3 t^2 + 4A_4 t^3 + 5A_5 t^4 + 6A_6 t^5 \quad (2)$$

The inflection point, which is the time at which there is a maximum change of calcium concentration (the rate is maximum), was obtained by equating the second derivative of eq 1 to zero

$$\frac{d^2 c(t)}{dt^2} = 2A_2 + 6A_3 t + 12A_4 t^2 + 20A_5 t^3 + 30A_6 t^4 = 0 \quad (3)$$

To determine the rate at the inflection point (r_{max}), the values of t and A_i from eq 3 were substituted into the rate formula in eq 2. The retardation efficiency (R) of each peptide was then calculated as

$$R = \frac{r_{control} - r_{max}}{r_{max}} \quad (4)$$

where $r_{control}$ corresponds to the maximum rate of the control group and r_{max} corresponds to that of each peptide group.

3. RESULTS AND DISCUSSION

3.1. Morphological Transformation during the Precipitation. Calcium phosphate was precipitated by a dropwise addition of phosphate salt solution into a calcium salt solution, in the absence or presence of oligo(L-glutamic acids) at a peptide concentration of 0.1 mM at room temperature and in a buffered system using HEPES at a pH of 7.4. Figure 1 shows the results of TEM analysis of precipitates at various time points from 2 min to 1 d. Morphologies for 2 and 10 min are similar to that for 30 min and are not shown. Several different morphologies are observed during the precipitation process. These distinct morphological features show that there are a few different precipitation stages occurring during calcium phosphate formation. Similar stages are observed in the absence or presence of glutamic acid peptides, though at

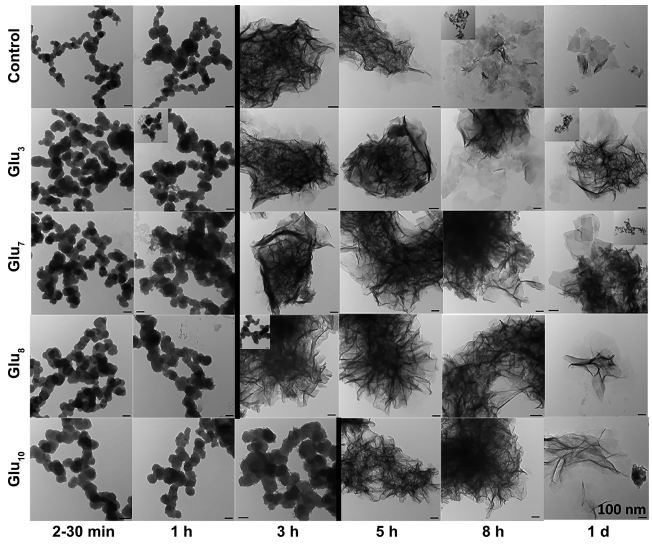

Figure 1. Morphological transformation of calcium phosphate precipitates formed in the absence or presence of 0.1 mM oligo(L-glutamic acids) observed over time by TEM. The black line indicates the time at which the spherical chain-like structures transform into a ribbon-like morphology.

https://dx.doi.org/10.1021/acs.jpcb.0c01689
J. Phys. Chem. B 2020, 124, 6278−6287

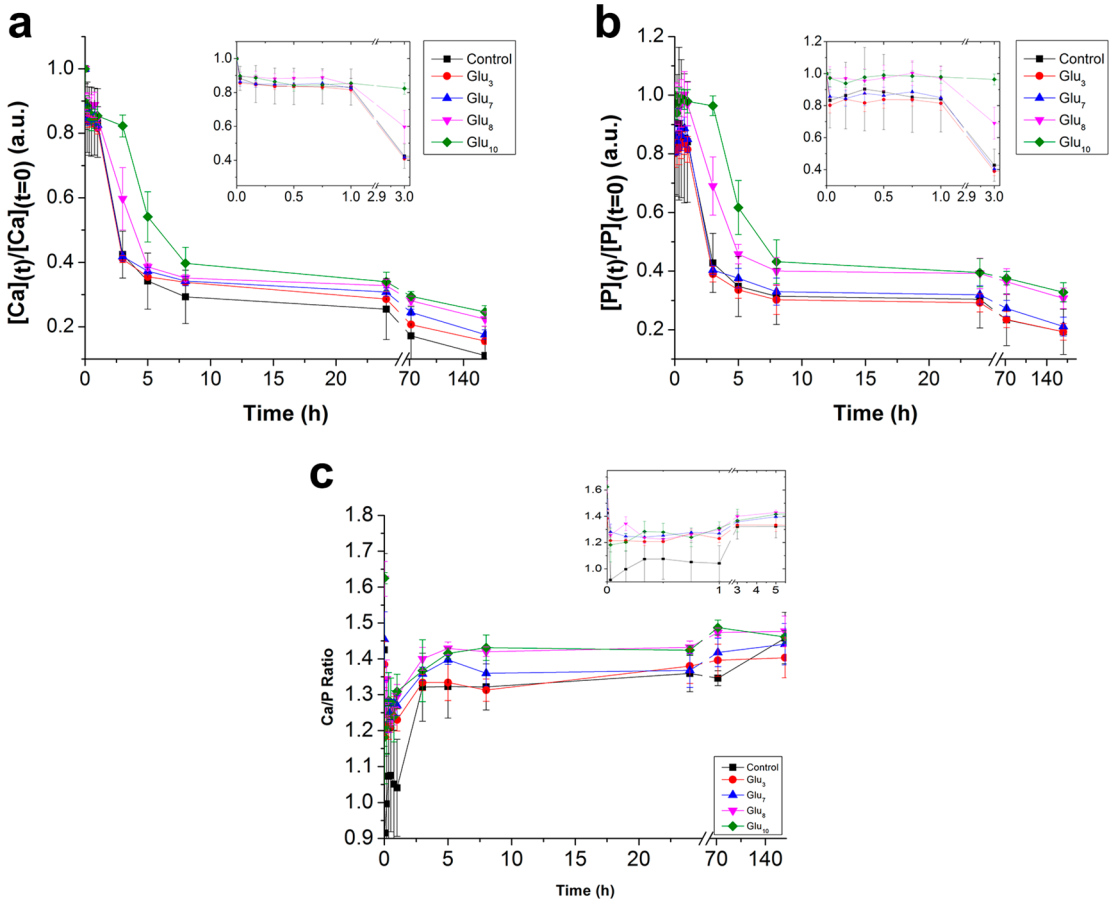

Figure 2. Relative calcium (a) and phosphate (b) concentrations in the supernatant normalized by each initial concentration, and Ca/P ratio of the precipitates (c) in the absence or presence of 0.1 mM oligo(L-glutamic acids) obtained ex situ using ICP-OES. Error bars are standard error from the average of three different experiments.

different time points. The first morphology observed within two minutes of reaction is the formation of subspherical particles measuring between 50 and 100 nm. These spheres are arranged in chain-like networks. These structures are hydrated, which is apparent from the appearance at higher magnification of porous structure within each sphere, indicative of beam damage. They aggregate to form macroscopically visible growing precipitates, which is supported by in situ dynamic light scattering (DLS) data (Figure S1). The formation of this structure has also been shown in several studies using a similar inorganic system.[15,23,28,34,35] One study assumed that this morphology is composed of highly hydrated spherulites of ACP joined together by secondary aggregation and that those spherulites are a result of primary aggregation of smaller primary particles.[23] In the control system without any peptides and in the systems of Glu_3, Glu_7, and Glu_8, these amorphous particles are seen up to 1 h of reaction. In contrast, the spheres are stable up to 3 h in the system with the longest peptide, Glu_{10}. These structures are seen in the control system as well as in the presence of all the peptides, suggesting that the peptides do not influence the nucleation of the ACP phase.

The chain-like structures then transform into ribbon-like morphology, which starts with the formation of spikes growing out on the surface of the spherical particles (Figure S2). The ribbons eventually evolve into a thin plate-like shape, showing the morphology of biomimetic apatite crystals.[15] During this period, the amorphous phase serves as a suitable template for nucleation of the crystalline phase by undergoing rearrangements through loss of water and ion ordering.[23,36] The transformation from spherical chain-like to a ribbon-like morphology in the control group occurs between 1 and 3 h, similar to what is observed in groups with Glu_3, Glu_7, and Glu_8. In Glu_{10}, however, this morphological transformation is delayed, and occurs between 3 and 5 h of reaction. This change is not merely a morphological transformation, but the precipitates also undergo a phase transition, as supported by SAED data (Figures S3a–S5a). Electron diffraction patterns show that the chain-like spherical structures are amorphous, indicated by the absence of any diffraction patterns either in the control group or in the systems with the shortest and longest peptides. By the time the ribbon-like morphology appears, however, SAED figures (Figures S3b–S5b) show the presence of diffraction rings that can be indexed as the HAP (002) and (112) faces. The presence of rings also indicates that the HAP nanocrystals were randomly oriented, and the HAP faces obtained in the peptide groups are the same as in the control. The TEM and SAED results thus far show that the crystallization proceeds through an ACP-mediated pathway, where precipitation starts with the initial formation of ACP followed by heterogeneous transformation to HAP at the ACP interface. The peptides do not influence the nucleation of the ACP phase and affect the phase transformation to HAP at a certain peptide chain length.

3.2. Solution Chemistry and Precipitation Kinetics. Throughout the reaction, the supernatant solution was taken at various time points and the concentrations of Ca and P ([Ca]

https://dx.doi.org/10.1021/acs.jpcb.0c01689
J. Phys. Chem. B 2020, 124, 6278–6287

and [P]) in the solution was determined using ICP-OES. In the first two minutes of the reaction, there is a sharp decrease of [Ca] and [P] in all groups, regardless of the presence of peptides, correlating to the observation of ACP spherical particles by TEM. This ICP-OES result further supports the fact that the peptides do not influence the nucleation of ACP. Another drastic drop in concentrations of both Ca and P is observed between 1 and 3 h in control, Glu_3, and Glu_7. The systems with Glu_8 and Glu_{10} experience two rapid drops, between 1 and 5 h and between 3 and 8 h, respectively. The transition time from spherical particles to the ribbon-like structure observed under TEM correlates well to the decrease in [Ca] and [P] in the supernatant solution for control, Glu_3, and Glu_7, and to the first sharp drop in concentrations for Glu_8 and Glu_{10} (Figure 2a,b). This result, again, indicates that each of the different morphologies characterizes a separate phase with its own representative calcium solubility, as also suggested by Habraken et al.[15] From both TEM and ICP-OES results, it is obvious that the glutamic acid trimer and heptamer show no influence on the precipitation of calcium phosphates, the octamer shows moderate influence, while the decamer shows the most significant ability to delay the transformation to crystalline phase up to 5 h compared to the inorganic control system. This phenomenon is similar to that found in the calcium oxalate system using different lengths of glutamic acid oligomer.[30] The current results imply that a certain length of glutamic acid peptide is needed to substantially delay the transformation of ACP to crystalline phase.

The precipitates obtained throughout the reaction were also analyzed using ICP-OES to measure the amounts of Ca and P present. The Ca/P ratio of the precipitates is shown in Figure 2c. In the earlier time points, between 2 min and 3 h (Figure 2c, inset), the Ca/P ratios start with a value of ~1.2 in all groups. As each group reaches the time where phase transformation occurs the Ca/P ratio increases sharply, a phenomenon complementary to what is observed in the supernatant. This time point, again, is associated with the morphological change observed by TEM. In different peptide groups, however, the Ca/P ratio values differ as the precipitate phase transforms. Control, Glu_3, and Glu_7 groups only reach a value of ~1.3, while Glu_8 and Glu_{10} are able to precipitate solids with Ca/P ratio up to ~1.45. Combined with the SAED data, this ratio indicates a formation of calcium-deficient apatite. The ratio obtained at the phase transformation only increases very slightly up to 7 d. These values suggest that there are intermediate stoichiometries, and the final phase will not be ideal HAP (stoichiometric Ca/P = 1.67), as observed similarly in a previous study using monolayers as a nucleation template.[37]

To further quantitate the kinetics of the different stages of precipitation, the change in $[Ca^{2+}]$ in solution was measured using Ca^{2+} ion-selective electrode in situ as a function of time. In detail, the exact time point at which the amorphous phase transitions into a more crystalline phase, the rate of the phase transformation and crystal growth, and the efficiency of each peptide group in retarding phase transformation was estimated. Figure 3 depicts the calcium ion concentration at each time point ($[Ca^{2+}]_t$) normalized by the maximum concentration ($[Ca^{2+}]_{max}$) in the absence or presence of glutamic acid peptides. The curve shows that the precipitation proceeds first through a period at which only a small concentration decrease occurs, followed by a second stage where there is a sharp drop in calcium concentration, and ends with a plateau where there

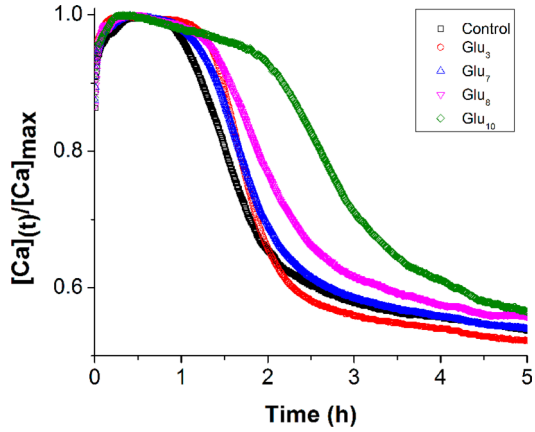

Figure 3. Relative Ca^{2+} concentration normalized to the maximum value in each group over time during calcium phosphate precipitation up to 5 h obtained by a Ca^{2+}-selective electrode in situ in the absence or presence of 0.1 mM oligo(L-glutamic acids). Each curve shown is the average of three individual experiments.

is only a small change in calcium concentration. The time at which the first period transitions to the second one in all groups was a little after 1 h, similar to the morphological transition between 1 and 3 h observed under TEM. The exception is seen with Glu_{10}, where the calcium ion concentration drops after 2 h. This time period for Glu_{10} does not exactly correlate to that obtained with TEM and ICP-OES, but it is expected, since TEM and ICP-OES were periodic measurements ex situ, while the Ca^{2+}-selective electrode is a continuous measurement and conducted in situ. Hence, the latter provides a continuous record and is very sensitive to the fluctuations in local ion concentration. The overall trend, however, corresponds well with the TEM and ICP-OES results in which only the longest peptide, Glu_{10}, delayed the ACP-mediated nucleation of HAP crystallites.

The induction time (t_i) is defined as the time elapsed when the nuclei of the crystalline phase are formed from the amorphous precursors. Table 1 summarizes the t_i values of

Table 1. Induction Time (t_i), Rate of Crystal Transformation and Growth (r_{max}), and Retardation Efficiency (R) of Peptides Obtained from Kinetics Experiment In Situ Using Ca^{2+}-selective Electrode[a]

group	t_i (h)	r_{max} (h^{-1})	R
Control	1.132 ± 0.156	0.367 ± 0.057	n/a
Glu_3	1.290 ± 0.026	0.364 ± 0.011	0.010 ± 0.029
Glu_7	1.236 ± 0.026	0.302 ± 0.006	0.179 ± 0.017
Glu_8	1.326 ± 0.111	0.267 ± 0.009	0.272 ± 0.024
Glu_{10}	1.956 ± 0.326	0.212 ± 0.006	0.424 ± 0.016

[a]Standard error was obtained from the average of three separate experiments

different groups. The Glu_3 and Glu_7 groups do not show any difference compared to the inorganic control. Glu_8, however, starts to show a longer t_i, indicating a delay of phase transition. Glu_{10} shows the longest t_i, almost double that of the control, demonstrating that it most efficiently retards the nucleation of the crystalline phase, a trend similar to that shown in the results of the above experiments.

Other than measuring t_i, the kinetics results also shed light on the rate of crystalline phase transformation and growth (r),

https://dx.doi.org/10.1021/acs.jpcb.0c01689
J. Phys. Chem. B 2020, 124, 6278−6287

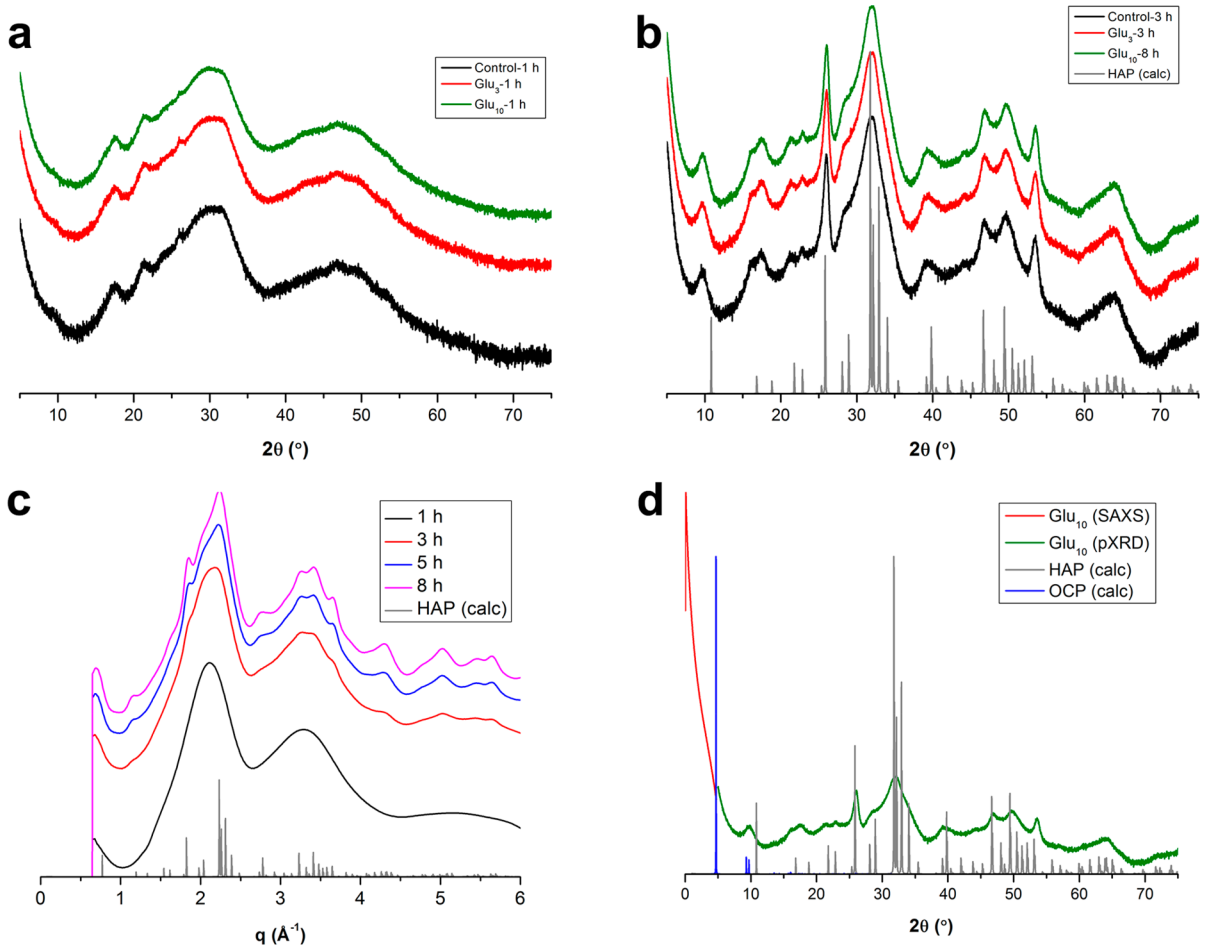

Figure 4. Powder XRD of precipitates in the absence or presence of 0.1 mM oligo(L-glutamic acids) at 1 h incubation (a) and at the phase transformation time (b). Synchrotron pXRD of precipitates in the presence of Glu_{10} at different incubation times (c). SAXS and pXRD data of precipitates in the presence of Glu_{10} at 8 h incubation time (d).

as well as the retardation efficiency (R) of the peptide. The rate calculation followed the methods previously reported by Fischer et al. for the calcium oxalate system.[30] The data in Table 1 show that the rate of transformation and growth with Glu_3 is similar to that in the absence of any peptide, as also shown by its R value of only 1%. As the chain length increases, however, the r_{max} decreases, a trend that is inversely correlated to both t_i and R. The Glu_{10} group slows down the transformation and growth up to ~42% with respect to control and represents the maximum retardation effect among all the peptide groups. The r_{max} values obtained indicate that glutamic acid peptides with a certain length influence calcium phosphate precipitation by decreasing the nucleation and growth rate of the crystalline phase. The mechanism may involve interaction between the carboxyl groups of the oligomer and calcium ions in solution or adsorption on/incorporation of this additive into the growing precipitate, or a combination of both. The results above show that, whatever the mechanism, there is an optimal length for the retardation effect at this low peptide concentration.

3.3. ACP-Mediated Phase Transformation. To better understand the phase transformation of the precipitate, the samples were analyzed by laboratory and synchrotron X-ray scattering methods. Control and groups with the shortest and longest peptides (Glu_3 and Glu_{10}) were selected for scattering experiments. Powder XRD (pXRD) data for precipitates at 1 h from these groups are shown in Figure 4a. The presence of a broad and diffuse XRD pattern at 2θ of ~30° indicates a lack of long-range order in the ACP precursor and confirms the previous TEM and SAED results. At later time points, more well-defined, albeit broadened, Bragg peaks appear at 2θ = 25° and 32°, which are in agreement with the calculated HAP reference peaks of the respective (002) and (211) planes (Figure 4b). These results indicate the transformation into a crystalline phase. Two peaks at 25° and 53° corresponding to (002) and (004) planes, respectively, are anomalously sharp, suggesting that the crystallites formed have a preferred growth direction along the direction of the c-axis. The timing of the increase in crystallinity is different for the different groups, with Glu_{10} being the slowest, starting at ~5 h (Figure S6). Powder XRD profiles of control, Glu_3, and Glu_{10} groups at different time points are shown in Figure S6.

Results of synchrotron pXRD for Glu_{10} with increasing incubation time are shown in Figure 4c, and pXRD profiles for control and Glu_3 are depicted in Figure S7. As described for the laboratory pXRD above, the increase in crystallinity in this sample is evidenced by the development of sharper Bragg peaks in the pXRD profile. The crystalline phase is again identified as HAP. The broadened nature of the HAP peaks suggests that the samples are composed of nanosized crystallites. The presence of OCP would be difficult to determine, as the main peak for this phase is at q = 0.34 $Å^{-1}$,

https://dx.doi.org/10.1021/acs.jpcb.0c01689
J. Phys. Chem. B 2020, 124, 6278−6287

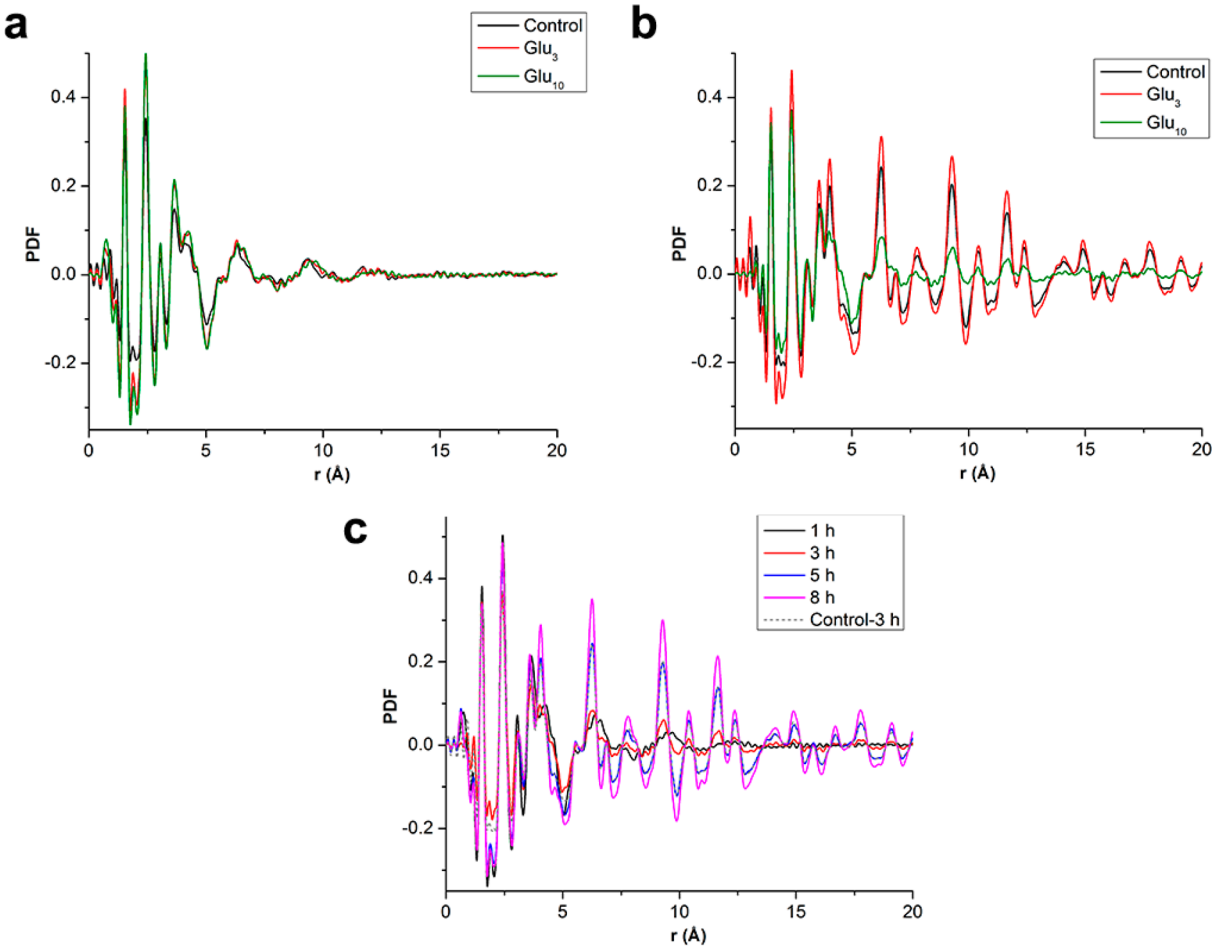

Figure 5. Comparison of PDFs for samples in the absence or presence of 0.1 mM peptides at incubation time of 1 h (a) and 3 h (b), and for samples in the presence of Glu_{10} at different incubation times (c).

which is less than the lowest resolvable angle in these synchrotron data ($q \approx 0.7$ Å^{-1}) because of the beam stop. To further clarify if OCP is present, observed SAXS and pXRD data for Glu_{10} at 8 h were plotted in one graph (Figure 4d). The pXRD peaks are generally in agreement with the calculated pattern of HAP. A broad peak observed at ∼10° 2θ tends to agree with peaks for both HAP and OCP, but the presence of OCP is still not definitive, since the much more intense peak of OCP for the (100) plane at ∼5° 2θ is not observed. The lack of a peak at ∼5° 2θ can also occur if the OCP is poorly crystalline, i.e., lacks periodic stacking of the layers.

Samples were also subjected to synchrotron X-ray scattering, and the data were analyzed to obtain pair distribution functions (PDF) to determine the local and medium range structure. At 1 h, PDF profiles show a small set of well-defined peaks at r < 10 Å indicating that precipitates in all groups have only short-range structural order (Figure 5a), consistent with the results from the previous experimental data. As described previously,[16,33] the individual peaks in the PDF can be assigned to one or more atom pairs in the ACP structure. For example, the first peak at approximately 1.53 Å corresponds to the average P−O distance in the phosphate group. Overall similarities in the positions and relative intensities of features in the PDF data suggest that the ACP precursors are structurally similar regardless of the presence or absence of peptides. The increase in crystallinity that occurs with sample aging is evidenced in the PDF by the appearance of new peaks at longer interatomic distances. For example, the control and Glu_3 samples show well-defined peaks up to and exceeding 20 Å by 3 h due to an increase in structural order caused by the transformation to HAP. In comparison, the precipitate with Glu_{10} remains mostly amorphous at 3 h due to the slower transformation kinetics. The PDFs for later time points for this sample eventually show similar changes, as it begins transforming into crystalline HAP by 5 h (Figure 5b,c). Quantification of the degree of transformation in the control and groups with the different peptide lengths is obtained from LCF. All groups show ACP as the most abundant phase (95−100%) at 1 h (Table 2). As the incubation proceeds to 3 h,

Table 2. Phase Abundance Estimation Using Linear Combination Fitting at Different Incubation Times in the Absence or Presence of 0.1 mM Oligo(L-glutamic acids)

group	time (h)	ACP	HAP
Control	1 h	95%	5%
Control	3 h	6%	94%
Glu_3	1 h	94%	6%
Glu_3	3 h	4%	96%
Glu_{10}	1 h	100%	0%
Glu_{10}	3 h	69%	31%
Glu_{10}	5 h	24%	76%
Glu_{10}	8 h	1%	99%

https://dx.doi.org/10.1021/acs.jpcb.0c01689
J. Phys. Chem. B 2020, 124, 6278−6287

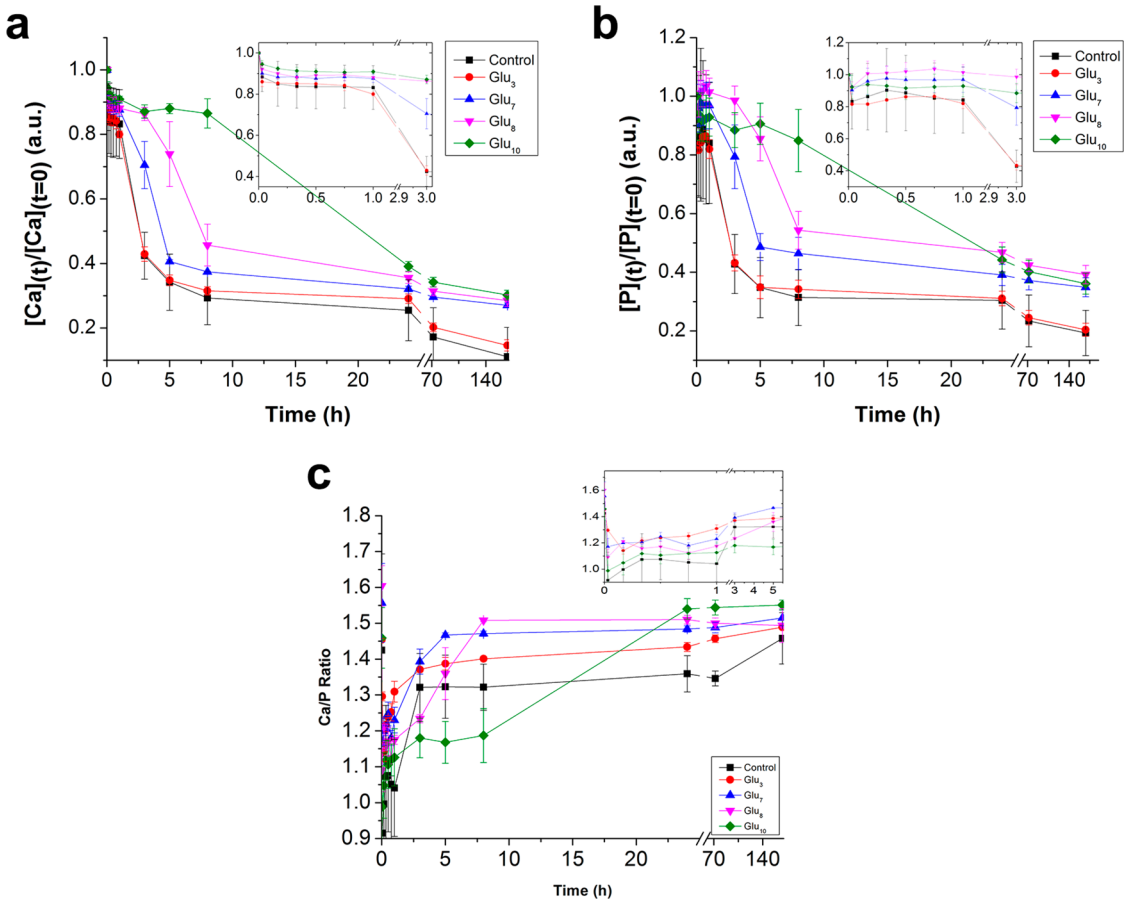

Figure 6. Relative calcium (a) and phosphate (b) concentrations in the supernatant normalized by each initial concentration, and Ca/P ratio of the precipitates (c) in the absence or presence of 0.5 mM oligo(L-glutamic acids) obtained using ICP-OES. Error bars are standard error from the average three different experiments.

however, control and Glu_3 groups have phase-transformed almost entirely to HAP, while the Glu_{10} group remains mostly amorphous. In agreement with Figure 5, the transformation of ACP in Glu_{10} is 76% complete by 5 h, and 100% completed by 8 h. Overall, all of the scattering data confirm a phase transition of ACP to HAP at different time periods depending on the different chain length of peptide.

3.4. Concentration of Oligo(L-glutamic acids). To determine the effect of the concentration of glutamic acid peptides on calcium phosphate precipitation, the same set of experiments (section 2.1) was carried out using 0.5 mM peptide, five times the concentration of the previous set of experiments. The precipitate morphology was characterized using TEM (Figure S8), and the solution as well as solid precipitate elemental analysis was obtained using ICP-OES (Figure 6). In all groups, the various morphological features are generally similar to those found using the lower peptide concentration. However, the timing of phase transformation is different compared to the lower concentration system for all groups, except for control and Glu_3(refer to black and white lines in Figure S8).

Using ICP-OES, the solution chemistry of the precipitates throughout the reaction was also analyzed (Figure 6). Similar to what is found using lower concentration of peptides, the time of the sharp drop in [Ca] and [P] in the supernatant (Figure 6a,b) is well-correlated with the time of phase transformation observed under TEM. The behavior observed for Glu_7 and Glu_8 indicates that there might be a critical concentration for each peptide chain length to retard phase transformation of calcium phosphate. The Ca/P ratios of the precipitates formed in the presence of 0.5 mM peptide (Figure 6c) explains the importance of the phase transformation delay mediated by peptides of different chain lengths in calcium phosphate precipitation. The Ca/P ratio of precipitates with the longest peptide, Glu_{10}, increases to a value of ~1.55, higher compared to those with shorter peptide chains. The slow uptake of calcium and phosphate from the supernatant mediated by Glu_{10} leads to precipitates with more perfect stoichiometry (closer to the Ca/P value of 1.67 for HAP) over a longer period of time.

4. CONCLUSIONS

In the present work, we investigate a series of well-defined lengths of negatively charged peptides, oligo(L-glutamic acids), in mediating calcium phosphate precipitation, utilizing different experimental techniques. Short glutamic acid peptides affect the precipitation of calcium phosphate by delaying the phase transformation of an ACP precursor to HAP. In the case of low concentration of peptide (0.1 mM), only the decamer of glutamic acids is optimal in delaying the phase transformation by slowing down the uptake of calcium and phosphate from the aqueous solution. The change in the kinetics of reaction by the longest peptide chain occurs by stabilization of the amorphous solid leading to an increase in the induction time for phase transformation to the crystalline phase and a decrease in the crystal growth rate. It is also found that a critical

https://dx.doi.org/10.1021/acs.jpcb.0c01689
J. Phys. Chem. B 2020, 124, 6278−6287

concentration of each peptide length is required to induce an effect on the precipitation kinetics. Finally, the retardation in phase transformation and crystal growth kinetics by longer oligopeptide results in a crystalline HAP with a stoichiometry closer to ideal. This work provides a systematic experimental investigation of HAP formation with the presence of short acidic peptide. The mechanism by which these short peptides mediate the calcium phosphate precipitation is explored in the second part of this series.[32]

■ ASSOCIATED CONTENT

Supporting Information

The Supporting Information is available free of charge at https://pubs.acs.org/doi/10.1021/acs.jpcb.0c01689.

DLS results, TEM images of the amorphous particle surface, SAED patterns, pXRD profiles, synchrotron pXRD profiles, TEM images of precipitates in the presence of 0.5 mM oligopeptide, and DLS experimental method (PDF)

■ AUTHOR INFORMATION

Corresponding Author

Nita Sahai − *Department of Polymer Science, Department of Geosciences, and Integrated Bioscience Program, The University of Akron, Akron, Ohio 44325, United States;* orcid.org/0000-0003-3852-0557; Email: sahai@uakron.edu

Authors

Putu Ustriyana − *Department of Polymer Science, The University of Akron, Akron, Ohio 44325, United States;* orcid.org/0000-0001-9804-3081

Emma Harmon − *Department of Polymer Science, The University of Akron, Akron, Ohio 44325, United States*

Kexun Chen − *Department of Polymer Science, The University of Akron, Akron, Ohio 44325, United States*

F. Marc Michel − *Department of Geosciences, Virginia Polytechnic Institute and State University, Blacksburg, Virginia 24061, United States*

Complete contact information is available at: https://pubs.acs.org/10.1021/acs.jpcb.0c01689

Notes

The authors declare no competing financial interest.

■ ACKNOWLEDGMENTS

We greatly acknowledge technical support on scattering experiments provided by the Virginia Tech National Center for Earth and Environmental Nanotechnology Infrastructure (NanoEarth) staff and the Virginia Tech Crystallography Lab (VTX). We are grateful for the technical assistance on SAED provided by Dr. Min Gao at the Advanced Materials and Liquid Crystal Institute, Kent State University, Kent, OH. We thank Dr. Michael Wilson and Dr. Saranshu Singla for the useful discussion in kinetics data analysis. We also appreciate the invaluable conversations with present and former members of the Sahai research group. We acknowledge financial support provided by start-up funds from The University of Akron and generous gift funds from Dr. Edward Weil to NS and The Robert Helm Jr. Fellowship in Polymers and Biomaterials awarded to PU. FMM gratefully acknowledges support provided by the National Science Foundation through CAREER-1652237. This research used resources of the Advanced Photon Source, a US Department of Energy (DOE) Office of Science User Facility operated for the DOE Office of Science by Argonne National Laboratory under Contract No. DE-AC02-06CH11357. Beamtime for the data collection presented in this paper was allocated under GUP 64554. This work was also supported by NanoEarth, a member of the National Nanotechnology Coordinated Infrastructure (NNCI), supported by NSF (ECCS 1542100).

■ REFERENCES

(1) Rodriguez, K.; Renneckar, S.; Gatenholm, P. Biomimetic Calcium Phosphate Crystal Mineralization on Electrospun Cellulose-Based Scaffolds. *ACS Appl. Mater. Interfaces* **2011**, *3*, 681−9.

(2) Li, X.; Xie, J.; Yuan, X.; Xia, Y. Coating Electrospun Poly(Epsilon-Caprolactone) Fibers with Gelatin and Calcium Phosphate and Their Use as Biomimetic Scaffolds for Bone Tissue Engineering. *Langmuir* **2008**, *24*, 14145−50.

(3) Yang, F.; Wolke, J. G. C.; Jansen, J. A. Biomimetic Calcium Phosphate Coating on Electrospun Poly(ε-Caprolactone) Scaffolds for Bone Tissue Engineering. *Chem. Eng. J.* **2008**, *137*, 154−161.

(4) Moritz, N.; Jokinen, M.; Peltola, T.; Areva, S.; Yli-Urpo, A. Local Induction of Calcium Phosphate Formation on TiO_2 Coatings on Titanium Via Surface Treatment with a CO_2 Laser. *J. Biomed. Mater. Res.* **2003**, *65*, 9−16.

(5) Roguska, A.; Pisarek, M.; Andrzejczuk, M.; Dolata, M.; Lewandowska, M.; Janik-Czachor, M. Characterization of a Calcium Phosphate- TiO_2 Nanotube Composite Layer for Biomedical Applications. *Mater. Sci. Eng., C* **2011**, *31*, 906−914.

(6) Habraken, W.; Habibovic, P.; Epple, M.; Bohner, M. Calcium Phosphates in Biomedical Applications: Materials for the Future? *Mater. Today* **2016**, *19*, 69−87.

(7) Stock, S. R. The Mineral-Collagen Interface in Bone. *Calcif. Tissue Int.* **2015**, *97*, 262−80.

(8) Sommerdijk, N. A.; Cusack, M. Biomineralization: Crystals Competing for Space. *Nat. Mater.* **2014**, *13*, 1078−9.

(9) Prasad Shastri, V. Biomineralization: A Confluence of Materials Science, Biophysics, Proteomics, and Evolutionary Biology. *MRS Bull.* **2015**, *40*, 473−477.

(10) George, A.; Veis, A. Phosphorylated Proteins and Control over Apatite Nucleation, Crystal Growth, and Inhibition. *Chem. Rev.* **2008**, *108*, 4670−4693.

(11) Mahamid, J.; Aichmayer, B.; Shimoni, E.; Ziblat, R.; Li, C.; Siegel, S.; Paris, O.; Fratzl, P.; Weiner, S.; Addadi, L. Mapping Amorphous Calcium Phosphate Transformation into Crystalline Mineral from the Cell to the Bone in Zebrafish Fin Rays. *Proc. Natl. Acad. Sci. U. S. A.* **2010**, *107*, 6316−6321.

(12) Mahamid, J.; Sharir, A.; Addadi, L.; Weiner, S. Amorphous Calcium Phosphate Is a Major Component of the Forming Fin Bones of Zebrafish: Indications for an Amorphous Precursor Phase. *Proc. Natl. Acad. Sci. U. S. A.* **2008**, *105*, 12748−53.

(13) Deshpande, A. S.; Beniash, E. Bioinspired Synthesis of Mineralized Collagen Fibrils. *Cryst. Growth Des.* **2008**, *8*, 3084−3090.

(14) Nudelman, F.; Pieterse, K.; George, A.; Bomans, P. H.; Friedrich, H.; Brylka, L. J.; Hilbers, P. A.; de With, G.; Sommerdijk, N. A. The Role of Collagen in Bone Apatite Formation in the Presence of Hydroxyapatite Nucleation Inhibitors. *Nat. Mater.* **2010**, *9*, 1004−1009.

(15) Habraken, W. J.; Tao, J.; Brylka, L. J.; Friedrich, H.; Bertinetti, L.; Schenk, A. S.; Verch, A.; Dmitrovic, V.; Bomans, P. H.; Frederik, P. M.; et al. Ion-Association Complexes Unite Classical and Non-Classical Theories for the Biomimetic Nucleation of Calcium Phosphate. *Nat. Commun.* **2013**, *4*, 1507.

(16) Posner, A. S.; Betts, F. Synthetic Amorphous Calcium Phosphate and Its Relation to Bone Mineral Structure. *Acc. Chem. Res.* **1975**, *8*, 273−281.

(17) Wang, L.; Nancollas, G. H. Pathways to Biomineralization and Biodemineralization of Calcium Phosphates: The Thermodynamic and Kinetic Controls. *Dalton Trans* **2009**, 2665−72.

(18) Wang, L.; Nancollas, G. H. Calcium Orthophosphates: Crystallization and Dissolution. *Chem. Rev.* **2008**, *108*, 4628−69.
(19) Hunter, G. K.; Goldberg, H. A. Modulation of Crystal Formation by Bone Phosphoproteins: Role of Glutamic Acid-Rich Sequences in the Nucleation of Hydroxyapatite by Bone Sialoprotein. *Biochem. J.* **1994**, *302*, 175−9.
(20) Hunter, G. K.; Goldberg, H. A. Nucleation of Hydroxyapatite by Bone Sialoprotein. *Proc. Natl. Acad. Sci. U. S. A.* **1993**, *90*, 8562−5.
(21) Boskey, A.; Maresca, M.; Ullrich, W.; Doty, S.; Butler, W.; Prince, C. Osteopontin-Hydroxyapatite Interactions in Vitro: Inhibition of Hydroxyapatite Formation and Growth in a Gelatin-Gel. *Bone Miner.* **1993**, *22*, 147−159.
(22) Hunter, G. K.; Kyle, C. L.; Goldberg, H. A. Modulation of Crystal Formation by Bone Phosphoproteins: Structural Specificity of the Osteopontin-Mediated Inhibition of Hydroxyapatite Formation. *Biochem. J.* **1994**, *300*, 723−8.
(23) Bar-Yosef Ofir, P.; Govrin-Lippman, R.; Garti, N.; Füredi-Milhofer, H. The Influence of Polyelectrolytes on the Formation and Phase Transformation of Amorphous Calcium Phosphate. *Cryst. Growth Des.* **2004**, *4*, 177−183.
(24) Diegmueller, J. J.; Cheng, X.; Akkus, O. Modulation of Hydroxyapatite Nanocrystal Size and Shape by Polyelectrolytic Peptides. *Cryst. Growth Des.* **2009**, *9*, 5220−5226.
(25) Tavafoghi, M.; Cerruti, M. The Role of Amino Acids in Hydroxyapatite Mineralization. *J. R. Soc., Interface* **2016**, *13*, 20160462.
(26) Tavafoghi Jahromi, M.; Cerruti, M. Amino Acid/Ion Aggregate Formation and Their Role in Hydroxyapatite Precipitation. *Cryst. Growth Des.* **2015**, *15*, 1096−1104.
(27) Jahromi, M. T.; Yao, G.; Cerruti, M. The Importance of Amino Acid Interactions in the Crystallization of Hydroxyapatite. *J. R. Soc., Interface* **2013**, *10*, 20120906.
(28) Jiang, S.; Pan, H.; Chen, Y.; Xu, X.; Tang, R. Amorphous Calcium Phosphate Phase-Mediated Crystal Nucleation Kinetics and Pathway. *Faraday Discuss.* **2015**, *179*, 451−61.
(29) Hentrich, D.; Junginger, M.; Bruns, M.; Börner, H. G.; Brandt, J.; Brezesinski, G.; Taubert, A. Interface-Controlled Calcium Phosphate Mineralization: Effect of Oligo(Aspartic Acid)-Rich Interfaces. *CrystEngComm* **2015**, *17*, 6901−6913.
(30) Fischer, V.; Landfester, K.; Muñoz-Espí, R. Stabilization of Calcium Oxalate Metastable Phases by Oligo(L-Glutamic Acid): Effect of Peptide Chain Length. *Cryst. Growth Des.* **2011**, *11*, 1880−1890.
(31) Elhadj, S.; Salter, E. A.; Wierzbicki, A.; De Yoreo, J. J.; Han, N.; Dove, P. M. Peptide Controls on Calcite Mineralization: Poly-aspartate Chain Length Affects Growth Kinetics and Acts as a Stereochemical Switch on Morphology. *Cryst. Growth Des.* **2006**, *6*, 197−201.
(32) Ustriyana, P.; Michel, F. M.; Wilson, M. C.; Harmon, E.; Chen, J.; Liu, T.; Sahai, N. Oligo(L-Glutamic Acids) in Calcium Phosphate Precipitation: Mechanism of Delayed Phase Transformation. *J. Phys. Chem. B* **2020**, 1 DOI: 10.1021/acs.jpcb.0c01690.
(33) Hoeher, A.; Mergelsberg, S.; Borkiewicz, O. J.; Dove, P. M.; Michel, F. M. A New Method for in Situ Structural Investigations of Nano-Sized Amorphous and Crystalline Materials Using Mixed-Flow Reactors. *Acta Crystallogr., Sect. A: Found. Adv.* **2019**, *75*, 758−765.
(34) Jiang, S.; Jin, W.; Wang, Y.-N.; Pan, H.; Sun, Z.; Tang, R. Effect of the Aggregation State of Amorphous Calcium Phosphate on Hydroxyapatite Nucleation Kinetics. *RSC Adv.* **2017**, *7*, 25497−25503.
(35) Tsuji, T.; Onuma, K.; Yamamoto, A.; Iijima, M.; Shiba, K. Direct Transformation from Amorphous to Crystalline Calcium Phosphate Facilitated by Motif-Programmed Artificial Proteins. *Proc. Natl. Acad. Sci. U. S. A.* **2008**, *105*, 16866−70.
(36) Brečević, L.; Hlady, V.; Füredi-Milhofer, H. Influence of Gelatin on the Precipitation of Amorphous Calcium Phosphate. *Colloids Surf.* **1987**, *28*, 301−313.
(37) Tarasevich, B. J.; Chusuei, C. C.; Allara, D. L. Nucleation and Growth of Calcium Phosphate from Physiological Solutions onto Self-Assembled Templates by a Solution-Formed Nucleus Mechanism. *J. Phys. Chem. B* **2003**, *107*, 10367−10377.

https://dx.doi.org/10.1021/acs.jpcb.0c01689
J. Phys. Chem. B 2020, 124, 6278−6287